RADAR STATIONARY AND MOVING INDOOR TARGET LOCALIZATION WITH LOW-RANK AND SPARSE REGULARIZATIONS

Van Ha Tang[‡] *Abdesselam Bouzerdoum*[⋆†] *Son Lam Phung*[⋆]

[‡]Faculty of Information Technology, Le Quy Don Technical University, Hanoi, Vietnam
[⋆]School of Electrical, Computer and Telecommunications Engineering,
University of Wollongong, Australia
[†]Division of Information and Computing Technology, College of Science and Engineering,
Hamad Bin Khalifa University, Doha, Qatar

ABSTRACT

This paper proposes a low-rank and sparse regularized optimization model to address the problem of wall clutter mitigation, stationary, and moving target indications using through-wall radar. The task of wall clutter suppression and target image reconstruction is formulated as a nuclear and ℓ_1 penalized least squares optimization problem in which the nuclear-norm term enforces for a low-rank wall clutter matrix and the ℓ_1-norm term promotes the sparsity of the target images. An iterative algorithm based on the proximal gradient technique is introduced to solve the optimization problem. The solution comprises the wall clutter and images of stationary and moving targets. Experiments are conducted on real radar data under compressive sensing scenarios. The results show that the proposed model is very effective at removing unwanted wall clutter, reconstructing stationary targets, and capturing moving targets.

***Index Terms*—** Through-the-wall radar imaging, moving target indication, wall clutter mitigation, compressive sensing.

1. INTRODUCTION

In urban sensing, through-wall radar imaging (TWRI) is a useful technology to image targets behind walls and other visually opaque materials. This capability has several potential applications in search-and-rescue, law-enforcement, and military operations [1]. In these applications, it is vital to provide high-resolution radar imaging of stationary and moving targets. This task, however, is difficult due to prolonged data collection and strong wall clutter [2–4]. To alleviate the burden of data collection, the problem of wall clutter mitigation, stationary, and moving target indications (MTI) needs to be tacked in the context of compressive sensing (CS) [5].

Several CS-based methods for radar imaging of stationary or moving indoor targets [6–11] mitigate wall clutter using background subtraction. The background subtraction effectively removes non-target clutter, but it relies on the access to a reference scene, which is unavailable for non-surveillance operations. To overcome this issue, multistage CS-based methods [12–15] first perform antenna signal estimation, then use a clutter mitigation technique, such as spatial filtering [2] or subspace projection [3] to estimate target signals, and finally reconstruct the target image. However, multistage processing could suffer from uncertainty and suboptimality of solution. Recent approaches perform wall clutter suppression and image reconstruction jointly, but these methods do not consider the problem of MTI in the imaging model [16, 17].

In general radar imaging of moving targets, Doppler processing, time-frequency representation, or change detection (CD) techniques can be used. For through-wall radar (TWR) sensing, however, changes in the phase of target signals do not necessarily lead to Doppler frequency shifts, making Doppler-processing ineffective [18, 19]. Time-frequency analysis is useful for regular motion detection, but it is complex to interpret TWR signals with non-homogeneous walls [20]. Therefore, CD was employed in several approaches for TWRI of moving targets [21–25]. The foundation of CD is that moving targets can be detected by subtracting successive datasets collected over several scans. In [21], MTI was obtained by applying CD to range profiles over consecutive datasets. In [22, 23], CD was applied to images formed using datasets collected at different time intervals. In the context of CS, CD was employed for removing stationary clutter, enabling the reconstruction of a sparse image of moving indoor targets [26, 20]. The combination of CD and CS allows MTI using reduced data, but CD suppresses also the stationary targets and thereby making them undetectable.

In this paper, wall clutter is captured using a low-rank regularization, and stationary and moving indoor targets are modeled using sparse representation. The task of wall clutter mitigation, stationary target reconstruction, and MTI is formulated as a composite nuclear-norm and ℓ_1-norm regularized least squares (LS) problem. To solve this problem efficiently, an iterative algorithm based on the proximal gradient technique is developed, capturing wall clutter and yielding a set of images of moving and stationary targets.

The remainder of the paper is organized as follows. Section 2 introduces the TWR signal model and discusses the combination of CS with CD techniques for MTI. Section 3 describes the optimization model for radar imaging of stationary and moving targets. Section 4 presents the experimental results. Finally, Section 5 gives concluding remarks.

2. TWR SIGNAL MODEL AND CD-BASED MTI

Consider a TWR system used to image targets behind a wall. To monitor moving targets, data collection is performed over I time intervals. At the ith interval, the radar imaging system uses N antennas and M narrowband signals to image the scene. Let $z_i(m,n)$ be the mth frequency radar signal received by the nth antenna for the ith interval. The signal $z_i(m,n)$ can be modeled as a superposition of the wall reflection $z_i^{\mathrm{w}}(m,n)$, stationary target return $z_i^{\mathrm{s}}(m,n)$,

The work of V. H. Tang is funded by Vietnam National Foundation for Science and Technology Development (NAFOSTED) under Grant 102.01-2017.307. The work of A. Bouzerdoum and S. L. Phung is supported by a grant from the Australian Research Council (ARC).

moving target echo $z_i^{\mathrm{m}}(m,n)$, and noise $v_i(m,n)$:

$$z_i(m,n) = z_i^{\mathrm{w}}(m,n) + z_i^{\mathrm{s}}(m,n) + z_i^{\mathrm{m}}(m,n) + v_i(m,n). \quad (1)$$

The wall component $z_i^{\mathrm{w}}(m,n)$ can be expressed as [12]

$$z_i^{\mathrm{w}}(m,n) = \sum_{r=1}^{R} \sigma_{\mathrm{w}} a_r e^{-j2\pi f_m \tau_{n,\mathrm{w}}^r}, \quad (2)$$

where σ_{w} is the reflectivity of the wall, R is the number of wall reverberations, a_r is the path loss factor of the rth wall return, and $\tau_{n,\mathrm{w}}^r$ is the propagation delay of the rth wall reverberation. The stationary target return is modeled as the superposition of P nonmoving target reflections [15]:

$$z_i^{\mathrm{s}}(m,n) = \sum_{p=1}^{P} \sigma_p e^{-j2\pi f_m \tau_{n,p}}, \quad (3)$$

where σ_p is the reflectivity of the pth target, and $\tau_{n,p}$ is the round-trip travel time of the signal from the nth antenna location to the pth target. The term $z_i^{\mathrm{m}}(m,n)$ is modeled as the superposition of Q moving targets:

$$z_i^{\mathrm{m}}(m,n) = \sum_{q=1}^{Q} \sigma_q^i e^{-j2\pi f_m \tau_{n,q}}, \quad (4)$$

where σ_q^i is the reflectivity of the qth target at the ith interval, and $\tau_{n,q}$ is the round-trip travel time of the signal from the nth antenna to the qth target. Note that the moving target appears stationary during the ith interval since it is a fraction of a second.

For image formation, the signal model in Eqs. (3) and (4) can be expressed in a vector-matrix form relating the signal to the target space. The indoor target space is partitioned into a rectangular grid consisting of L pixels along the crossrange and downrange. Let $s_i^{\mathrm{s}}(l)$ and $s_i^{\mathrm{m}}(l)$ denote weighted indicator functions representing the pth stationary and the qth moving target reflectivities, respectively. The functions $s_i^{\mathrm{s}}(l)$ and $s_i^{\mathrm{m}}(l)$ are defined as

$$s_i^{\mathrm{s}}(l) = \begin{cases} \sigma_p, & \tau_{n,l} = \tau_{n,p}, \\ 0, & \tau_{n,l} \neq \tau_{n,p}, \end{cases} \quad (5)$$

$$s_i^{\mathrm{m}}(l) = \begin{cases} \sigma_q^i, & \tau_{n,l} = \tau_{n,q}, \\ 0, & \tau_{n,l} \neq \tau_{n,q}. \end{cases} \quad (6)$$

Eqs. (5) and (6) imply that the value of the lth pixel is nonzero if it includes either the pth stationary or the qth moving target. Here, $\tau_{n,l}$ is the focusing delay between the nth antenna and the lth pixel. From Eqs. (3) and (4), we can rearrange the stationary target signal $\mathbf{z}_{i,n}^{\mathrm{s}} = [z_i^{\mathrm{s}}(1,n), \ldots, z_i^{\mathrm{s}}(M,n)]^T$ and the moving target return $\mathbf{z}_{i,n}^{\mathrm{m}} = [z_i^{\mathrm{m}}(1,n), \ldots, z_i^{\mathrm{m}}(M,n)]^T$ for M frequencies. Thus, the signal model can be expressed

$$\mathbf{z}_{i,n}^{\mathrm{s}} = \mathbf{\Psi}_n \, \mathbf{s}_i^{\mathrm{s}}, \quad \mathbf{z}_{i,n}^{\mathrm{m}} = \mathbf{\Psi}_n \, \mathbf{s}_i^{\mathrm{m}}. \quad (7)$$

Here, $\mathbf{\Psi}_n$ is an $M \times L$ matrix with the (m,l)th entry given by $\psi_n(m,l) = \exp(-j2\pi f_m \tau_{n,l})$, $\mathbf{s}_i^{\mathrm{s}} = [s_i^{\mathrm{s}}(1), \ldots, s_i^{\mathrm{s}}(L)]^T$, and $\mathbf{s}_i^{\mathrm{m}} = [s_i^{\mathrm{m}}(1), \ldots, s_i^{\mathrm{m}}(L)]^T$. Stacking measurements for N antennas $\mathbf{z}_i^{\mathrm{s}} = [(\mathbf{z}_{i,1}^{\mathrm{s}})^T, \ldots, (\mathbf{z}_{i,N}^{\mathrm{s}})^T]^T$, and $\mathbf{z}_i^{\mathrm{m}} = [(\mathbf{z}_{i,1}^{\mathrm{m}})^T, \ldots, (\mathbf{z}_{i,N}^{\mathrm{m}})^T]^T$, we can express

$$\mathbf{z}_i^{\mathrm{s}} = \mathbf{\Psi} \, \mathbf{s}_i^{\mathrm{s}}, \quad \mathbf{z}_i^{\mathrm{m}} = \mathbf{\Psi} \, \mathbf{s}_i^{\mathrm{m}}, \quad (8)$$

where $\mathbf{\Psi} = [\mathbf{\Psi}_1^T, \ldots, \mathbf{\Psi}_N^T]^T$. It follows from (1) and (8) that

$$\mathbf{z}_i = \mathbf{z}_i^{\mathrm{w}} + \mathbf{\Psi} \, \mathbf{s}_i^{\mathrm{s}} + \mathbf{\Psi} \, \mathbf{s}_i^{\mathrm{m}} + \boldsymbol{\upsilon}_i. \quad (9)$$

For MTI, CD can be applied to the successive datasets $\{\mathbf{z}_i\}$ to remove stationary components. Let $\bar{\mathbf{z}}_i$ denote a difference vector between $\mathbf{z}_{i+1}$ and $\mathbf{z}_i$, for $i = 1 \ldots, I-1$. From (9), we have

$$\bar{\mathbf{z}}_i = \mathbf{z}_{i+1} - \mathbf{z}_i = \mathbf{\Psi} \, \bar{\mathbf{s}}_i + \bar{\boldsymbol{\upsilon}}_i, \quad (10)$$

where $\bar{\mathbf{s}}_i = \mathbf{s}_{i+1}^{\mathrm{m}} - \mathbf{s}_i^{\mathrm{m}}$, and $\bar{\boldsymbol{\upsilon}}_i = \boldsymbol{\upsilon}_{i+1} - \boldsymbol{\upsilon}_i$. Here, the stationary components, $\mathbf{z}_i^{\mathrm{w}}$ and $\mathbf{\Psi}\mathbf{s}_i^{\mathrm{s}}$, are assumed to be identical between consecutive intervals, and hence they are removed. The resultant vector $\bar{\mathbf{z}}_i$ is used to reconstruct $\bar{\mathbf{s}}_i$, which represents target movements from the ith to $(i+1)$th intervals. Exploiting sparsity of $\bar{\mathbf{s}}_i$, the moving target image can be obtained by solving the following optimization problem,

$$\min_{\bar{\mathbf{s}}_i} \quad \|\bar{\mathbf{s}}_i\|_1 \quad \text{subject to} \quad \|\bar{\mathbf{z}}_i - \mathbf{\Psi} \, \bar{\mathbf{s}}_i\|_2^2 \leq \epsilon, \quad (11)$$

where ϵ is a noise bound. An efficient approach considers solving this problem in the Lagrangian form:

$$\bar{\mathbf{s}}_i = \arg\min_{\bar{\mathbf{s}}_i} \frac{1}{2} \|\bar{\mathbf{z}}_i - \mathbf{\Psi} \, \bar{\mathbf{s}}_i\|_2^2 + \lambda \, \|\bar{\mathbf{s}}_i\|_1, \quad (12)$$

where λ is a positive parameter used to trade off between the LS and the ℓ_1 penalty terms. Convex analysis theory proves that Problems (11) and (12) are equivalent [27], provided that ϵ and λ obey certain relationships.

It is worth noting that CD mitigates background clutter and enables a sparse image of moving indoor targets to be reconstructed [19, 20, 26]. However, this CD-based model is greedy in that it removes also stationary targets. Furthermore, it is evident from (12) that the combination of CD and CS processes the ith dataset $\bar{\mathbf{z}}_i$ to recover the ith interval image independently, employing only ℓ_1 regularizer. To overcome these issues, this paper introduces an optimization model that captures wall clutter and indicates stationary and moving targets simultaneously.

3. LOW-RANK AND SPARSE REGULARIZED LS MODEL

The proposed optimization model is described in the next subsection, followed by an iterative solver developed based on the proximal gradient (PG) technique in Subsection 3.2.

3.1. Nuclear-norm and ℓ_1-norm Regularized LS Problem

Let $\mathbf{Z}_i = [z_i(m,n)]$, $\mathbf{Z}_i^{\mathrm{w}} = [z_i^{\mathrm{w}}(m,n)]$, $\mathbf{Z}_i^{\mathrm{s}} = [z_i^{\mathrm{s}}(m,n)]$, $\mathbf{Z}_i^{\mathrm{m}} = [z_i^{\mathrm{m}}(m,n)]$, and $\mathbf{\Upsilon}_i = [v_i(m,n)]$ denote the $M \times N$ matrices containing, respectively, the radar signals, the wall reflections, stationary target returns, moving target signals, and the noise received for all M frequencies by all N antennas at the ith interval. Equation (1) can be rewritten in a matrix form as

$$\mathbf{Z}_i = \mathbf{Z}_i^{\mathrm{w}} + \mathbf{Z}_i^{\mathrm{s}} + \mathbf{Z}_i^{\mathrm{m}} + \mathbf{\Upsilon}_i. \quad (13)$$

In a CS scenario, only a reduced subset of K measurements ($K \ll M \times N$) is collected at each interval. Let $\mathbf{\Phi} \in \mathbb{R}^{K \times MN}$ denote a sensing matrix in which each row has only one non-zero element (equal to 1) indicating the selected frequency for a particular antenna. The relation between the compressed measurement vector $\mathbf{y}_i \in \mathbb{C}^K$ and the full matrix $\mathbf{Z}_i$ can be expressed as

$$\mathbf{y}_i = \mathbf{\Phi} \, \mathrm{vec}(\mathbf{Z}_i) = \mathbf{\Phi} \, \mathrm{vec}(\mathbf{Z}_i^{\mathrm{w}} + \mathbf{Z}_i^{\mathrm{s}} + \mathbf{Z}_i^{\mathrm{m}} + \mathbf{\Upsilon}_i), \quad (14)$$

where $\mathrm{vec}(\mathbf{Z}_i)$ denotes the vectorization operator stacking the columns of $\mathbf{Z}_i$ into a composite column vector. Note that $\mathbf{Z}_i$ can be

obtained from $\mathbf{y}_i$ as $\mathbf{Z}_i = \mathrm{mat}(\mathbf{\Phi}^\dagger\, \mathbf{y}_i)$, where mat denotes the operator reshaping a column vector of MN elements into an $M \times N$ matrix, and † denotes the pseudo-inverse operator. Exploiting the relation between the target measurements and the image given in (8), it follows from Eq. (14) that

$$\mathbf{y}_i = \mathbf{\Phi}\ [\mathrm{vec}(\mathbf{Z}_i^{\mathrm{w}}) + \mathbf{\Psi}\ \mathbf{s}_i + \mathrm{vec}(\mathbf{\Upsilon}_i)]\,, \tag{15}$$

where $\mathbf{s}_i = \mathbf{s}_i^{\mathrm{s}} + \mathbf{s}_i^{\mathrm{m}}$. This implies that $\mathbf{s}_i$ represents both stationary and moving targets present at the ith interval.

Now, we arrange all the measurement sets along the I intervals into a matrix $\mathbf{Y} = [\mathbf{y}_1, \ldots, \mathbf{y}_I]$, and the wall reflections into a matrix $\mathbf{Z}^{\mathrm{w}} = [\mathbf{Z}_1^{\mathrm{w}}, \ldots, \mathbf{Z}_I^{\mathrm{w}}]$, we can obtain the image of both stationary and moving targets $\mathbf{S} = [\mathbf{s}_1, \ldots, \mathbf{s}_I]$ by solving the following optimization problem:

$$\begin{aligned} \min_{\mathbf{Z}^{\mathrm{w}},\mathbf{S}} \quad & \|\mathbf{Z}^{\mathrm{w}}\|_* + \lambda\, \|\mathbf{S}\|_1 \\ \text{subject to} \quad & \|\mathbf{Y} - [\mathcal{A}(\mathbf{Z}^{\mathrm{w}}) + \mathbf{\Phi}\ \mathbf{\Psi}\ \mathbf{S}]\|_F^2 \le \epsilon. \end{aligned} \tag{16}$$

Here, $\|\mathbf{Z}^{\mathrm{w}}\|_*$ denotes the nuclear-norm defined as the sum of the singular values of the matrix, $\|\mathbf{Z}^{\mathrm{w}}\|_* = \sum_{j=1}^{J} \sigma_j(\mathbf{Z}^{\mathrm{w}})$ with $\sigma_j(\mathbf{Z}^{\mathrm{w}})$ being the jth largest singular value of matrix $\mathbf{Z}^{\mathrm{w}}$ of rank at most J, $\|\mathbf{S}\|_1$ is the ℓ_1-norm of matrix $\mathbf{S}$ computed as the sum of the absolute entries $\|\mathbf{S}\|_1 = \sum_l \sum_i |S(l,i)|$, λ is the regularization parameter reflecting a trade-off between the low-rank and sparse terms, $\|\cdot\|_F$ denotes the Frobenius norm, ϵ is a noise bound, and the operator $\mathcal{A}(\mathbf{Z}^{\mathrm{w}})$ is defined as $\mathcal{A}(\mathbf{Z}^{\mathrm{w}}) = [\mathbf{\Phi}\ \mathrm{vec}(\mathbf{Z}_1^{\mathrm{w}}), \ldots, \mathbf{\Phi}\ \mathrm{vec}(\mathbf{Z}_L^{\mathrm{w}})]$. To solve Problem (16) efficiently, we cast it into the Lagrangian form:

$$\begin{aligned} \min_{\mathbf{Z}^{\mathrm{w}},\mathbf{S}} f(\mathbf{Z}^{\mathrm{w}}, \mathbf{S}) = \frac{1}{2}\, \|\mathbf{Y} - [\mathcal{A}(\mathbf{Z}^{\mathrm{w}}) + \mathbf{\Phi}\ \mathbf{\Psi}\ \mathbf{S}]\|_F^2 \\ + \gamma(\|\mathbf{Z}^{\mathrm{w}}\|_* + \lambda\, \|\mathbf{S}\|_1), \end{aligned} \tag{17}$$

where γ is a positive parameter. Now the task is to minimize $f(\mathbf{Z}^{\mathrm{w}}, \mathbf{S})$ to solve for the wall clutter $\mathbf{Z}^{\mathrm{w}}$ and target image $\mathbf{S}$ jointly.

3.2. Iterative Proximal Gradient Algorithm

This subsection presents an iterative algorithm based on PG technique [28–30] to solve Problem (17). PG considers solving the problem with an objective function:

$$\min_{\mathbf{x}} f(\mathbf{x}) = g(\mathbf{x}) + \lambda\, h(\mathbf{x}), \tag{18}$$

where $g(\mathbf{x})$ is convex, differentiable, and smooth, e.g., the quadratic term in (17), and $h(\mathbf{x})$ is convex but not necessary smooth, e.g., the sum of the nuclear and ℓ_1 norms in (17). Satisfying these conditions, Problem (18) is solved efficiently using an iterative technique. Let $\mathbf{x}_k$ denote an estimate of the solution at the k-th iteration. Then, the next estimate of the minimizer is obtained by solving:

$$\mathbf{x}_{k+1} = \arg\min_{\mathbf{x}} \frac{1}{2}\, \|\mathbf{a}_k - \mathbf{x}\|_2^2 + \lambda\alpha\, h(\mathbf{x}), \tag{19}$$

where the auxiliary variable $\mathbf{a}_k$ is defined as

$$\mathbf{a}_k = \mathbf{x}_k - \alpha \nabla g(\mathbf{x}_k). \tag{20}$$

Here, $\nabla g(\mathbf{x}_k)$ denotes the gradient of $g(\mathbf{x})$ evaluated at the current estimate $\mathbf{x}_k$. When ∇g is a Lipschitz continuous function with constant C, this method converges if $\alpha \in (0,\ 1/C]$.

We use the PG scheme to solve Problem (17). Minimizing $f(\mathbf{Z}^{\mathrm{w}}, \mathbf{S})$ generates a sequence of estimates for the wall component $\mathbf{Z}^{\mathrm{w}}$ and target image $\mathbf{S}$. Let $\{\mathbf{Z}_k^{\mathrm{w}}, \mathbf{S}_k\}$ denote an estimate at the kth iteration. Defining an adjoint operator $\mathcal{A}^*(\mathbf{Y})$ as $\mathcal{A}^*(\mathbf{Y}) = [\mathrm{mat}(\mathbf{\Phi}^\dagger\, \mathbf{y}_1), \ldots, \mathrm{mat}(\mathbf{\Phi}^\dagger\, \mathbf{y}_I)]$, the next estimate $\{\mathbf{Z}_{k+1}^{\mathrm{w}}, \mathbf{S}_{k+1}\}$ is obtained by solving

$$\begin{aligned} (\mathbf{Z}_{k+1}^{\mathrm{w}}, \mathbf{S}_{k+1}) = \arg\min_{\mathbf{Z}^{\mathrm{w}},\mathbf{S}} \frac{1}{2}\|\mathbf{Z}_k - \mathbf{Z}^{\mathrm{w}} - \mathcal{A}^*(\mathbf{\Phi}\mathbf{\Psi}\mathbf{S})\|_F^2 \\ + \alpha\gamma\|\mathbf{Z}^{\mathrm{w}}\|_* + \alpha\, \gamma\, \lambda\, \|\mathbf{S}\|_1, \end{aligned} \tag{21}$$

where $\mathbf{Z}_k$, playing the role of $\mathbf{a}_k$ in (20), is evaluated by

$$\mathbf{Z}_k = \mathbf{Z}_k^{\mathrm{w}} + \mathcal{A}^*(\mathbf{\Phi}\ \mathbf{\Psi}\ \mathbf{S}_k) - \alpha\mathcal{A}^*(\mathcal{A}(\mathbf{Z}_k^{\mathrm{w}}) + \mathbf{\Phi}\ \mathbf{\Psi}\ \mathbf{S}_k - \mathbf{Y}). \tag{22}$$

Since the variables $\mathbf{Z}^{\mathrm{w}}$ and $\mathbf{S}$ are separable, Problem (21) is minimized by solving two subproblems:

$$\mathbf{Z}_{k+1}^{\mathrm{w}} = \arg\min_{\mathbf{Z}^{\mathrm{w}}} \frac{1}{2}\|\mathbf{Z}_k - \mathbf{Z}^{\mathrm{w}} - \mathcal{A}^*(\mathbf{\Phi}\mathbf{\Psi}\mathbf{S}_k)\|_F^2 + \alpha\gamma\|\mathbf{Z}^{\mathrm{w}}\|_*, \tag{23}$$

$$\mathbf{S}_{k+1} = \arg\min_{\mathbf{S}} \frac{1}{2}\|\mathbf{Z}_k - \mathbf{Z}_{k+1}^{\mathrm{w}} - \mathcal{A}^*(\mathbf{\Phi}\mathbf{\Psi}\mathbf{S})\|_F^2 + \alpha\gamma\lambda\|\mathbf{S}\|_1. \tag{24}$$

The task now is to solve Subproblems (23) and (24). The nuclear-norm regularized LS problem in (23) can be solved efficiently using the *singular value soft-thresholding* (SVT) technique [31]. The solution is given by applying SVT to the input matrix $[\mathbf{Z}_k - \mathcal{A}^*(\mathbf{\Phi}\ \mathbf{\Psi}\ \mathbf{S}_k)]$:

$$\mathbf{Z}_{k+1}^{\mathrm{w}} = \mathcal{S}_{\alpha\gamma}(\mathbf{Z}_k - \mathcal{A}^*(\mathbf{\Phi}\ \mathbf{\Psi}\ \mathbf{S}_k)). \tag{25}$$

Given the singular value decomposition of $\mathbf{Z}$ as $\mathbf{Z} = \mathbf{U}\,\mathbf{\Lambda}\,\mathbf{V}^H$, SVT operator $\mathcal{S}_\tau(\mathbf{Z})$ is defined by $\mathcal{S}_\tau(\mathbf{Z}) = \mathbf{U}\ \mathcal{T}_\tau(\mathbf{\Lambda})\ \mathbf{V}^H$. Here the soft-thresholding operator $\mathcal{T}_\tau(x)$ is computed as

$$\mathcal{T}_\tau(x) = \mathrm{sgn}(x)\max(|x| - \tau, 0) = \frac{x}{|x|}\max(|x| - \tau, 0). \tag{26}$$

Note that for vectors or matrices, the soft-thresholding operator $\mathcal{T}_\tau(\cdot)$ is applied to each element (entrywise).

The ℓ_1-norm penalized LS problem in (24) can be handled using the generic PG decomposition in Eqs. (19) and (20):

$$\mathbf{S}_{k+1} = \arg\min_{\mathbf{S}} \frac{1}{2}\, \|\mathbf{X} - \mathbf{S}\|_F^2 + \beta\alpha\gamma\lambda\, \|\mathbf{S}\|_1\,, \tag{27}$$

where the auxiliary variable $\mathbf{X}$ is computed as

$$\mathbf{X} = \mathbf{S}_k - \beta\mathbf{\Psi}^H\, [\mathbf{\Psi}\ \mathbf{S}_k - (\mathbf{Z}_k - \mathbf{Z}_{k+1}^{\mathrm{w}})]\,. \tag{28}$$

Here, the parameter β satisfies $\beta \in (0, 1/||\mathbf{\Psi}||_2^2]$ for convergence. The solution to Problem (27) is given by applying the shrinkage operator $\mathcal{T}(\cdot)$ in (26) to the auxiliary variable $\mathbf{X}$ in (28):

$$\mathbf{S}_{k+1} = \mathcal{T}_{\beta\alpha\gamma\lambda}(\mathbf{X}). \tag{29}$$

Table 1 provides the iterative steps to solve Problem (17). The input includes data matrix $\mathbf{Y}$, parameters α, β, γ, λ, and a tolerance tol. The parameters α and β are gradient stepsizes; they are set to the largest possible values for fast convergence, whereas the parameters γ and λ are problem-dependent and need to be tuned appropriately. The algorithm performs two major tasks: wall-component estimation (Step 3) and target image reconstruction (Step 4). The algorithm stops when it converges to a local optimum. Here, it terminates if the relative change of the objective function is negligible (see Step 5). Note that the ith column in $\mathbf{S}$ represents the targets present at the ith interval. To monitor the moving target trajectory, we can combine all I images and form a composite map $\mathbf{s}$ as

$$s(l) = \max_i |s_i(l)|,\ \text{for } i = 1, \ldots, I. \tag{30}$$

Table 1. Algorithm 1: Iterative estimations of wall clutter, stationary and moving indoor target images.

1) Initialize $\mathbf{Z}_0^{\mathrm{w}} \leftarrow \mathcal{A}^*(\mathbf{Y})$, $\mathbf{S}_0 \leftarrow \mathbf{0}$, $k \leftarrow 0$.
2) Perform gradient decomposition using (22):
$\mathbf{Z}_k \leftarrow \mathbf{Z}_k^{\mathrm{w}} + \mathcal{A}^*(\mathbf{\Phi}\ \mathbf{\Psi}\ \mathbf{S}_k) - \alpha\mathcal{A}^*(\mathcal{A}(\mathbf{Z}_k^{\mathrm{w}}) + \mathbf{\Phi}\ \mathbf{\Psi}\ \mathbf{S}_k - \mathbf{Y})$.
3) Estimate wall component using (25):
$\mathbf{Z}_{k+1}^{\mathrm{w}} \leftarrow \mathcal{S}_{\alpha\gamma}(\mathbf{Z}_k - \mathcal{A}^*(\mathbf{\Phi}\ \mathbf{\Psi}\ \mathbf{S}_k))$.
4) Estimate target images using (28) and (29):
$\mathbf{X} \leftarrow \mathbf{S}_k - \beta\mathbf{\Psi}^H[\mathbf{\Psi}\ \mathbf{S}_k - (\mathbf{Z}_k - \mathbf{Z}_{k+1}^{\mathrm{w}})]$,
$\mathbf{S}_{k+1} \leftarrow \mathcal{T}_{\beta\alpha\gamma\lambda}(\mathbf{X})$.
5) Evaluate the cost function $f(\mathbf{Z}_{k+1}^{\mathrm{w}}, \mathbf{S}_{k+1})$ using (17).
If $\frac{|f(\mathbf{Z}_{k+1}^{\mathrm{w}}, \mathbf{S}_{k+1}) - f(\mathbf{Z}_k^{\mathrm{w}}, \mathbf{S}_k)|}{|f(\mathbf{Z}_k^{\mathrm{w}}, \mathbf{S}_k)|} < \mathrm{tol}$, then terminate algorithm, otherwise increment $k \leftarrow k+1$, and go back to Step 2.

4. EXPERIMENTAL RESULTS

The proposed model was evaluated using real radar datasets collected from the Imaging Laboratory at the University of Wollongong, NSW, Australia. A synthetic aperture radar (SAR) system was setup to image a scene containing a 0.16 m thick wooden wall, a 0.2 m triangular plate trihedral, and a 0.2 m square plate dihedral. During data acquisition, the trihedral target remains stationary and the dihedral target moves along a trajectory indicated by Pos. 1 to Pos. 3, as shown in Fig. 1. The SAR transceives a stepped-frequency signal comprising 801 frequencies, equispaced over 2 GHz bandwidth centered at 2.0 GHz with 2.5 MHz frequency step. The aperture array has 61 elements, with an inter-element spacing of 0.01 m. The radar system was placed at a standoff distance of 1.0 m from the wall. Data were collected for three intervals, starting with the dihedral target at Pos. 1 and ending with the dihedral target at Pos. 3.

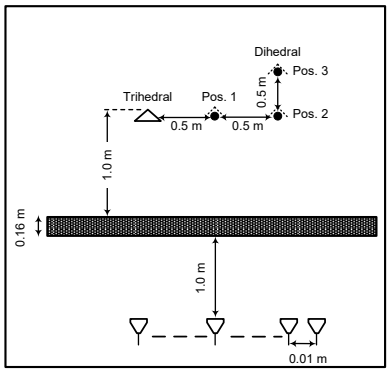

Fig. 1. Layout of the TWRI scene comprising both stationary and moving targets.

The proposed iterative algorithm requires a set of input parameters, which were chosen as follows. The gradient stepsize parameters α and β were set to $\alpha = 1/\|\mathbf{\Phi}\|_2^2$ and $\beta = 1/\|\mathbf{\Psi}\|_2^2$ for accelerated convergence. The regularization parameters γ and λ need to be tuned appropriately. Here in the experiments, they were chosen as $\gamma = 10^{-1}\|\mathcal{A}^*(\mathbf{Y})\|_2$ and $\lambda = 0.25\max\{\|(\mathbf{\Phi\Psi})^H\mathbf{y}_i\|_\infty\}_{i=1}^I$. The tolerance was set to $\mathrm{tol} = 10^{-4}$.

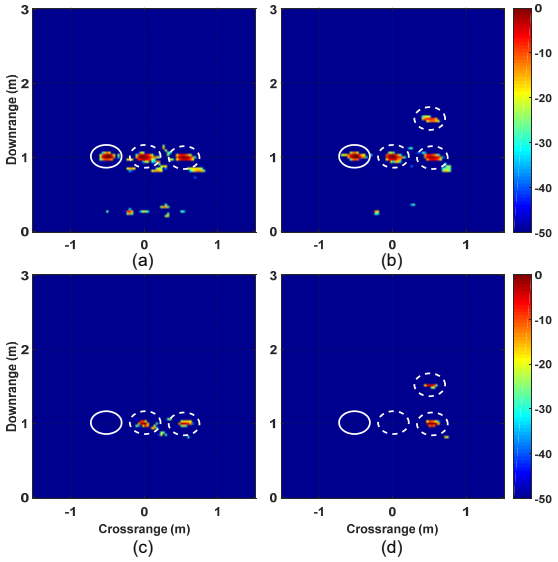

Fig. 2. Target images reconstructed by different methods with 50% frequencies and 50% antennas: (a) proposed method using the first and second datasets, (b) proposed method using the first, second, and third datasets, (c) CD & ℓ_1 min. applied to the first and second datasets, and (d) CD & ℓ_1 min. applied to the second and third datasets. The stationary target is indicated by a solid circle, and the trajectory of moving target is indicated by dashed circles.

Clutter mitigation and target image reconstruction were performed using reduced datasets generated by randomly selecting 50% (400 out of 801) of the total frequencies at half the antenna locations (31 out of 61) selected randomly. Fig. 2 shows the composite target images $\mathbf{s}$ obtained by progressively reconstructing target images. Fig. 2(a) shows the target image formed by the proposed model using the first and second interval datasets. The stationary and moving targets are localized at their positions. Fig. 2(b) presents the target image formed by the proposed method with three datasets. The stationary indoor target is detected and the moving target is indicated along its trajectory. Furthermore, we notice that when more datasets are combined, the quality of clutter mitigation and target reconstruction is enhanced. The existing two-stage approach, CD followed by ℓ_1 minimization [19, 20, 26] was implemented on the same datasets. Fig. 2(c) shows target image formed after subtracting the first dataset from the second dataset. The moving target is localized at Pos. 1 and 2, but the stationary target is suppressed. Applying CD to the second and third datasets can detect the moving target, but CD again removes the stationary target, as demonstrated in Fig. 2(d).

5. CONCLUSION

This paper presented a low-rank and sparse penalized LS optimization model for solving the problem of clutter mitigation and image reconstruction of stationary and moving indoor targets in compressive TWRI. Through experimental validation, we find that the proposed model segregates wall clutter from target reflections well and enables the detection of both stationary and moving targets, even with reduced measurements. Furthermore, by processing several datasets progressively, the proposed model enhances the level of clutter mitigation and target image reconstruction.

6. REFERENCES

[1] M. G. Amin (Ed.), *Through-The-Wall Radar Imaging*. Boca Raton, FL: CRC Press, 2010.

[2] Y.-S. Yoon and M. G. Amin, "Spatial filtering for wall-clutter mitigation in through-the-wall radar imaging," *IEEE Trans. Geosci. and Remote Sens.*, vol. 47, no. 9, pp. 3192–3208, Sept. 2009.

[3] F. H. C. Tivive, A. Bouzerdoum, and M. G. Amin, "A subspace projection approach for wall clutter mitigation in through-the-wall radar imaging," *IEEE Trans. Geosci. and Remote Sens.*, vol. 53, no. 4, pp. 2108–2122, Apr. 2015.

[4] V. H. Tang, A. Bouzerdoum, S. L. Phung, and F. H. C. Tivive, "A sparse Bayesian learning approach for through-wall radar imaging of stationary targets," *IEEE Trans. Aerosp. and Electron. Syst.*, vol. 53, no. 5, pp. 2485–2501, Oct. 2017.

[5] D. L. Donoho, "Compressed sensing," *IEEE Trans. Inf. Theory*, vol. 52, no. 4, pp. 1289–1306, Apr. 2006.

[6] Y.-S. Yoon and M. G. Amin, "Compressed sensing technique for high-resolution radar imaging," in *Proc. SPIE: Signal Process., Sensor Fusion, and Target Recognition XVII*, Orlando, FL, Mar. 2008, pp. 69 681A.1– 69 681A.10.

[7] Q. Huang, L. Qu, B. Wu, and G. Fang, "UWB through-wall imaging based on compressive sensing," *IEEE Trans. Geosci. and Remote Sens.*, vol. 48, no. 3, pp. 1408–1415, Mar. 2010.

[8] M. Leigsnering, C. Debes, and A. M. Zoubir, "Compressive sensing in through-the-wall radar imaging," *Proc. IEEE Int. Conf. Acoust., Speech, and Signal Process.*, pp. 4008–4011, Prague, Czech Republic, 22–27 May 2011.

[9] V. H. Tang, A. Bouzerdoum, and S. L. Phung, "Two-stage through-the-wall radar image formation using compressive sensing," *J. Electron. Imaging*, vol. 22, no. 2, pp. 021006-1 – 021006-10, Apr.–Jun. 2013.

[10] J. Qian, F. Ahmad, and M. G. Amin, "Joint localization of stationary and moving targets behind walls using sparse scene recovery," *J. Electron. Imaging*, vol. 22, no. 2, pp. 021002-1 – 021002-10, Apr.–Jun. 2013.

[11] M. Leigsnering, F. Ahmad, M. G. Amin, and A. M. Zoubir, "Compressive sensing-based multipath exploitation for stationary and moving indoor target localization," *IEEE J. Selected Topics in Signal Process.*, vol. 9, no. 8, pp. 1469 – 1483, Dec. 2015.

[12] E. Lagunas, M. G. Amin, F. Ahmad, and M. Najar, "Joint wall mitigation and compressive sensing for indoor image reconstruction," *IEEE Trans. Geosci. and Remote Sens.*, vol. 51, no. 2, pp. 891 – 906, Feb. 2013.

[13] V. H. Tang, A. Bouzerdoum, S. L. Phung, and F. H. C. Tivive, "Enhanced wall clutter mitigation for through-the-wall radar imaging using joint Bayesian sparse signal recovery," *Proc. IEEE Int. Conf. Acoust., Speech and Signal Process.*, pp. 7804–7808, Florence, Italy, May 2014.

[14] A. Bouzerdoum, F. H. C. Tivive, and V. H. Tang, "Multi-polarization through-the-wall radar imaging using joint Bayesian compressed sensing," in *IEEE Int. Conf. Digital Signal Process.*, Hong Kong, Aug. 2014, pp. 783–788.

[15] F. Ahmad, J. Qian, and M. G. Amin, "Wall clutter mitigation using discrete prolate spheroidal sequences for sparse reconstruction of indoor stationary scenes," *IEEE Trans. Geosci. and Remote Sens.*, vol. 53, no. 3, pp. 1549–1557, Mar. 2015.

[16] V. H. Tang, A. Bouzerdoum, S. L. Phung, and F. H. C. Tivive, "Radar imaging of stationary indoor targets using joint low-rank and sparsity constraints," in *IEEE Int. Conf. Acoust., Speech and Signal Process.*, Shanghai China, Mar. 2016, pp. 1412–1416.

[17] V. H. Tang, A. Bouzerdoum, and S. L. Phung, "Multipolarization through-wall radar imaging using low-rank and jointly-sparse representations," *IEEE Trans. Image Process.*, vol. 27, no. 4, pp. 1763–1776, Apr. 2018.

[18] M. G. Amin and F. Ahmad, "Change detection analysis of humans moving behind walls," *IEEE Trans. Aerosp. and Electron. Syst.*, vol. 49, no. 3, pp. 1410–1425, Jul. 2013.

[19] M. G. Amin, "Sparsity-aware human motion indication," in *Compressive Sensing for Urban Radar*. M. G. Amin (Ed.), Boca Raton, FL: CRC Press, Aug. 2014, pp. 251–282.

[20] F. Ahmad and M. G. Amin, "Through-the-wall human motion indication using sparsity-driven change detection," *IEEE Trans. Geosci. and Remote Sens.*, vol. 51, no. 2, pp. 881–890, Feb. 2013.

[21] K. Ranney et al., "Recent MTI experiments using ARL's synchronous impulse reconstruction (SIRE) radar," in *Proc. SPIE Radar Sensor Technology XII*, Apr. 2008, pp. 694 708–1–694 708–9.

[22] J. Moulton et al., "Target and change detection in synthetic aperture radar sensing of urban structures," in *IEEE Radar Conf.*, Rome Italy, May 2008.

[23] F. Soldovieri, R. Solimene, and R. Pierri, "A simple strategy to detect changes in through the wall imaging," *Progress in Electromagnetics Research M*, vol. 7, pp. 1–13, 2009.

[24] A. R. Hunt, "Use of a frequency-hopping radar for imaging and motion detection through walls," *IEEE Trans. Geosci. and Remote Sens.*, vol. 47, no. 5, pp. 1402–1408, May 2009.

[25] Y. D. Zhang and A. Hunt, "Image and localization of behind-the-wall targets using collocated and distributed apertures," in *Through-the-Wall Radar Imaging*. M. G. Amin (Ed.), Boca Raton, FL: CRC Press, 2010, pp. 122–154.

[26] M. G. Amin, F. Ahmad, and W. Zhang, "A compressive sensing approach to moving target indication for urban sensing," in *Proc. IEEE Radar Conf.*, Kansas City, USA, May 2011, pp. 509–512.

[27] R. T. Rockafellar, *Convex Analysis*. Princeton Math. Ser. 28, Princeton University Press, Princeton, NJ, 1970.

[28] P. L. Combettes and V. R. Wajs, "Signal recovery by proximal forward-backward splitting," *SIAM J. Multiscale Modeling Simulation*, vol. 4, no. 4, pp. 1168–1200, Nov. 2006.

[29] S. J. Wright, R. D. Nowak, and M. A. T. Figueiredo, "Sparse reconstruction by separable approximation," *IEEE Trans. Signal Process.*, vol. 57, no. 7, pp. 2479–2493, Jul. 2009.

[30] N. Parikh and S. Boyd, "Proximal algorithms," in *Found. and Trends in Optimization*, vol. 1, no. 3. Now Publishers Inc, Nov. 2013, pp. 123–231.

[31] J.-F. Cai, E. J. Candes, and Z. Shen, "A singular value thresholding algorithm for matrix completion," *SIAM J. Optimization*, vol. 20, no. 4, pp. 1956–1982, Mar. 2010.